Optical spin sorting chain

Hinamoto, Tatsuki
Fujii, Minoru
Sannomiya, Takumi

(Citation)
Optics Express,29(22):34951-34961

(Issue Date)
2021-10-25

(Resource Type)
journal article

(Version)
Version of Record

Research Article | Vol. 29, No. 22 / 25 Oct 2021 / Optics Express 34951
Optics EXPRESS

Optical spin sorting chain

TATSUKI HINAMOTO,[1,3] MINORU FUJII,[1] AND TAKUMI SANNOMIYA[2,4]

[1]Department of Electrical and Electronic Engineering, Graduate School of Engineering, Kobe University, Rokkodai, Nada, Kobe 657-8501, Japan
[2]Department of Materials Science and Technology, Tokyo Institute of Technology, 4259 Nagatsuta Midoriku, Yokohama 226-8503, Japan
[3]tatsuki.hinamoto@gmail.com
[4]sannomiya.t.aa@m.titech.ac.jp

Abstract: Transverse spin angular momentum of light is a key concept in recent nanophotonics to realize unidirectional light transport in waveguides by spin-momentum locking. Herein we theoretically propose subwavelength nanoparticle chain waveguides that efficiently sort optical spins with engineerable spin density distributions. By arranging high-refractive-index nanospheres or nanodisks of different sizes in a zigzag manner, directional optical spin propagation is realized. The origin of efficient spin transport is revealed by analyzing the dispersion relation and spin angular momentum density distributions, being attributed to guided modes that possess transverse spin angular momenta. In contrast to conventional waveguides, the proposed asymmetric waveguide can spatially separate up- and down-spins and locate one parity inside and the other outside the structure. Moreover, robustness against bending the waveguide and its application as an optical spin sorter are presented. Compared to previous reports on spatial engineering of local spins in photonic crystal waveguides, we achieved miniaturization of the entire footprint down to the subwavelength scale.

1. Introduction

Advances in the field of nanophotonics have paved the way toward highly integrated photonic circuits by miniaturizing optical components. Recently, recognition of the spin-momentum locking (SML) of light, in analogy to the quantum spin Hall effect, is revolutionizing the field. [1] SML is the key concept of chiral light-matter interactions, where the direction of momentum is fundamentally locked by the polarization state of light. [2] Using this idea, spin-photon interfaces are now capable of uniquely determining the information transfer direction from or to a quantum emitter according to its spin. There are versatile fields that gain benefits from chiral light-matter interactions, ranging from valleytronics and chiral sensing to quantum information processing. [3,4] In particular, quantum network designs would be substantially accelerated through the development of basic device elements that work as qubits, memories, nodes, paths, routers, isolators, and so on.

SML is a universal phenomenon accompanied by evanescent waves; [2] in principle, no complicated structures are required to realize chiral interactions. Indeed, SML has been demonstrated in various photonic structures, such as metal surfaces [5–7], fibers [8], strips [9–11], and photonic crystal waveguides [12,13]. In such symmetric one-dimensional (1D) waveguides, SML is typically achieved by positioning an individual scatterer beneath the waveguides or by embedding or placing a light source (*e.g.,* quantum dots) at a position offset from the propagation so that spins with different parities have different spatial or energetical distribution. This however requires sophisticated and accurate positioning of the emitter since the spin densities are equally distributed in the same material and a slight displacement in the material can flip the SML direction. On the other hand, in the case of photonic crystal waveguides, the local spins in the

#437725 https://doi.org/10.1364/OE.437725
Journal © 2021 Received 18 Jul 2021; revised 18 Sep 2021; accepted 1 Oct 2021; published 11 Oct 2021

Optics EXPRESS

waveguide itself have been spatially engineered. [12] Although its large degree of freedom to engineer optical properties is useful, the two-dimensional (2D) nature of photonic crystals can be a limitation in highly integrated photonic circuits since the entire footprints spanning over dozens of periods (typically $>10\lambda$) are required to constitute photonic bands.

Herein, we propose a novel 1D waveguide in the form of a chain, which can miniaturize the SML waveguides with engineerable spin densities down to a subwavelength scale. The design of the waveguide stems from linearly aligned 1D nanoparticle chains made of high-index dielectrics. In such dielectric chain structures, it is known that light propagates with low loss (*e.g.* ~5 dB/mm [14]) by couplings of Mie resonances resulting from the confinement of light within each nanoparticle. [14–22] They are one of the promising waveguides because of various prominent features: bending stability to 90° corner [19], all-optical modulation with a response time of 50 ps [16], and slow light with group velocity down to 0.03 of the speed of light [17]. Our idea in this work is to introduce asymmetry to the 1D chain waveguide by a side chain to realize an SML waveguide that spatially separates up and down local spins predominantly inside and outside waveguides. In contrast to conventional 1D waveguide geometries, the spatial distributions of local spins can be tailored by simple structural parameters, such as the particle size, position, and gap. Furthermore, the discontinuous nature of the chain structure offers a facile connection to various functional photonic components including isolators and routers, which we also demonstrate in this work.

In this paper, we first demonstrate the unidirectional light transmission in the asymmetric zigzag chain with a representative structure. The structure is then optimized by tuning the asymmetry of the system, that is, the size of the side chain. We then reveal the mechanism of the unidirectional transmission by analyzing the dispersion relation as well as the spin angular momentum (SAM) density distribution, which elucidates how SML and the efficient coupling of a circular dipole source are realized. Finally, we exhibit the functionalities and applications of the proposed system.

2. Results and discussion

Figure 1(a) schematically visualizes the concept of this work. The proposed waveguide consists of silicon nanospheres of different sizes linearly arranged in a zigzag manner and is excited with a circularly polarized dipole to mimic a quantum dot that has circular polarization states. To study the SML in the chain, we simulate its optical properties using the finite-difference time-domain (FDTD) method. The simulation model is shown in Fig. 1(b). Silicon spheres with radii R_1 and R_2 are aligned with a fixed gap length g. The number of large spheres (N) is fixed to 31, if not specified. The circular dipole is composed of linearly polarized two dipoles oriented along x- and y-axes, respectively. By setting a $\pi/2$-phase difference between these orthogonal dipoles, the source has $\sigma^{\pm}$ polarizations ($p = p_0(x \pm iy)e^{i\omega t}$). At first, the source is situated at the center of a larger sphere at the middle of the chain (the 16th sphere when $N = 31$). The spin-sorting performance of the chain is evaluated by light transmission at the rightmost (T_R) and leftmost (T_L) spheres. Note that T_R and T_L have been normalized by the net power coupled to the waveguide. We define a starter structural parameter set (R_1, R_2, g) = (120 nm, 80 nm, 5 nm), which we call the "basic parameter set". These spheres have the dipolar Mie resonances (*i.e.*, electric and magnetic dipole modes) around the red to near-infrared spectral range. Further details of the simulation method are provided in the Methods section.

Figure 1(c) (bottom panel) shows transmission spectra for an asymmetric zigzag chain with the basic structural parameter set under excitation with a σ^- dipole. The spectra show different spectral responses between the right (blue) and left (red) side propagations. For example, it indicates that ~40% of coupled light propagates to the right in the wavelength range of 0.7–0.8 μm (≡ the first band), while less than 10% reach the left side. In the wavelength above 0.93 μm (≡ the second band) opposite behavior is observed, that is, the light preferentially propagates to the

Optics EXPRESS

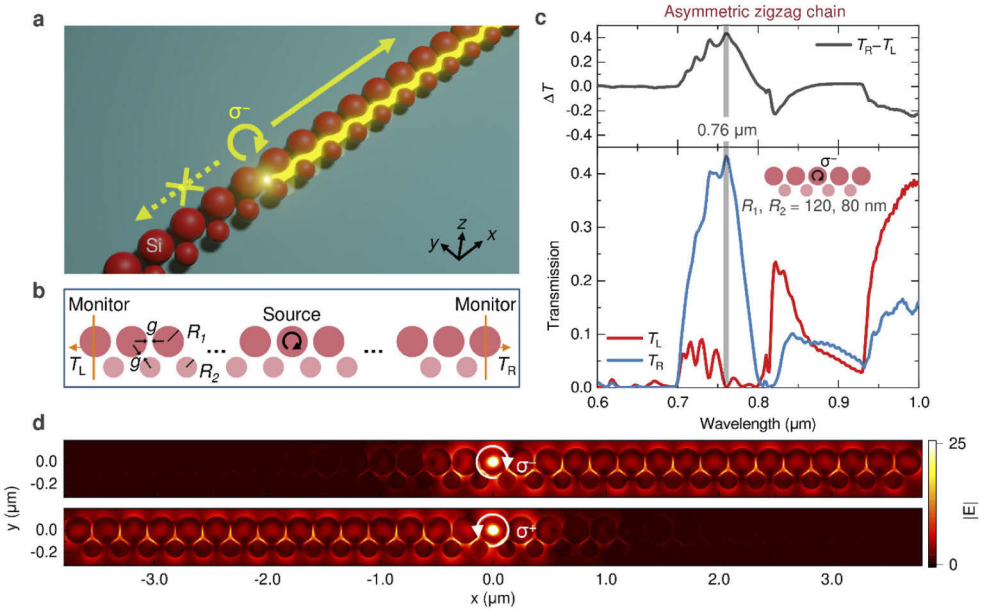

Fig. 1. Concept of the proposed asymmetric zigzag chain waveguide. (a) Schematic illustration. (b) Simulation configuration for the waveguide consisting of silicon nanospheres. (c) Light transmission under the excitation with a σ^- dipole. Transmission spectra in the right (T_R; blue curve) and left (T_L; red curve) direction are shown on the bottom. The difference $\Delta T = T_R - T_L$ is shown on the top. (d) Electric field distributions at the wavelength of 0.76 μm under σ^- (top) and $\sigma+$ (bottom) dipole excitation. The calculations in panels c and d are performed with the basic parameter set of $(R_1, R_2, g) = (120\text{ nm}, 80\text{ nm}, 5\text{ nm})$.

left. The difference of the transmission, $\Delta T = T_R - T_L$, is plotted in the top panel, showing the higher selectivity in the first band. The highest contrast is observed at the wavelength of 0.76 μm. Note that the highest ΔT wavelength slightly differs depending on N because of the formation of a band within a finite number of periods (Fig. S1). Even after averaging the transmission over N (*i.e.*, N dependent factors are eliminated), 97% of the transmitted light reaches the right at the highest ΔT wavelength. Besides, the operating wavelength can be readily tuned by the sphere size because of the scaling nature of the Mie resonance (Fig. S2). An electric field profile at $\lambda = 0.76$ μm is shown on the top panel of Fig. 1(d) and clearly depicts the unidirectional propagation of light towards the right without significant decay. Because the system does not break time-reversal symmetry, the propagating direction can be switched oppositely under σ^+ dipole excitation as shown on the bottom panel. These behaviors unambiguously evidence the existence of SML. Such spin-dependent light transport can also be explained as the optical spin-Hall effect since inversion symmetry is absent in the system. [23]

We also notice that the propagation loss $1 - (T_R + T_L)$ is not negligible. There are two possible dissipation channels: absorption and radiative losses. Silicon has some material absorption loss in the visible range, which decreases at longer wavelengths. In fact, T_R and T_L increase as the operating wavelength red-shifts (see Fig. S2). A certain radiative loss also exists for such chain waveguides. The radiative loss is likely to increase when a high-index substrate exists. Although such losses can be higher than photonic crystal waveguides, the small footprint can be useful for many applications. It is worth noting that the propagation loss of dielectric chains (up to ~ 5 dB/mm [14]) is, in general, much lower than plasmonic counterparts (*e.g.*, ~1 dB/50 nm [24]).

Optics EXPRESS

Before the detailed analysis of the unidirectional spin-dependent light transport, we now find the optimal structure by phenomenologically studying the size effect of the side chain. Figure 2 presents the side chain size (R_2) dependence of the transmission spectrum with a fixed large chain size ($R_1 = 120$ nm) and gap length ($g = 5$ nm). Figure 2(a) and (b) show two-dimensional (2D) transmission maps when R_2 is changed from 0 nm (a linear 1D chain without the side chain) to 120 nm ($R_1 = R_2$, that is, an symmetric zigzag chain). The corresponding 2D map of ΔT is shown in Fig. 2(c). We see that in the first band ($\lambda = 0.7$ to 0.8 μm) the SML arises ($\Delta T \sim +0.5$) at around $R_2 = 80$ nm, corresponding to the radius ratio $R_2 / R_1 \sim 0.66$, while the opposite parity SML appears ($\Delta T \sim -0.5$) above $R_2 = 90$ nm in the second band ($\lambda > 0.93$ μm).

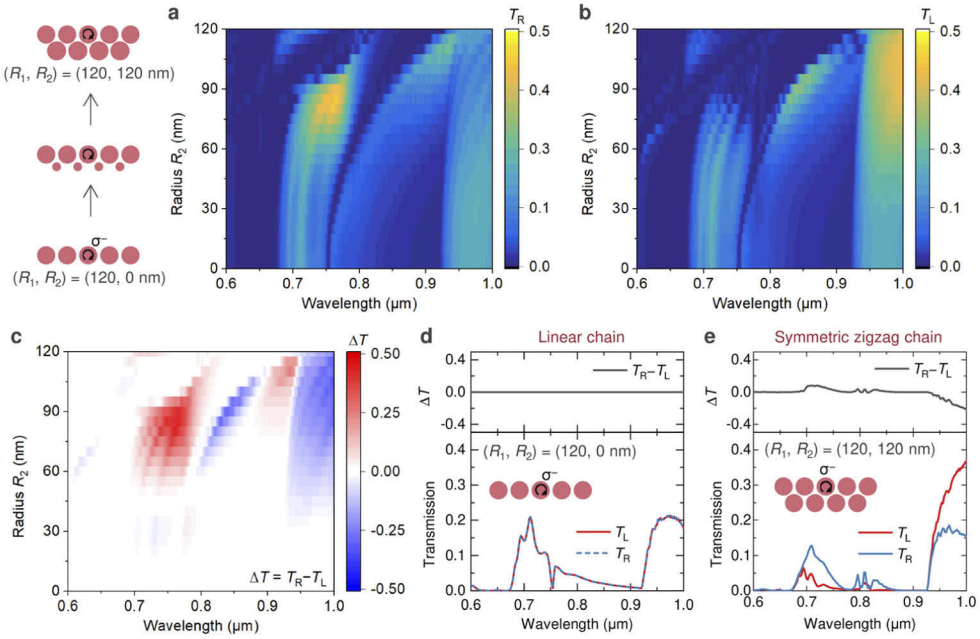

Fig. 2. Radius ratio-dependent light propagation in the asymmetric zigzag chain waveguide for R_2 from 0 to120 nm (R_1 and g are fixed to 120 and 5 nm, respectively). (a,b) Transmission on the (a) right and (b) left edges and (c) transmission difference $\Delta T = T_R - T_L$. Transmission spectra of (d) the linear chain and (e) the symmetric zigzag chain. The plots in panels d and e correspond to the profiles in panels a-c at $R_2 = 0$ and 120 nm, respectively. The excitation dipole is a σ^- dipole excitation in all cases.

For more detailed analysis, the transmission spectra of the symmetric waveguides, *i.e.*, the linear ($R_2 = 0$ nm) and the symmetric zigzag chains ($R_2 = 120$ nm), are extracted and plotted in Fig. 2(d) and (e), respectively. In the case of the linear chain, T_R and T_L are identical because of its symmetry. The first and second transmission bands are still observed around 0.7 and 1.0 μm, with a slight blue-shift compared to the basic structure shown in Fig. 1. We notice that a sum of the peak values ($T_R + T_L \sim 0.4$) is equivalent to the peak T_R (first band) or T_L (second band) of the asymmetric zigzag chain (Fig. 1(c)). This means that adding the side chain does not degrade the transmission efficiency. In the symmetric zigzag chain (Fig. 2(e)), we see significantly degraded transmission in the first band. In this configuration, the directionality originates from the asymmetrically positioned excitation source. [9] Although the total transmission is comparable to the asymmetric zigzag chain for the second band, the ΔT (~ -0.2) is much smaller than the asymmetric chain. As another example of structural design, the gap length dependence is provided in Supplement 1 (Fig. S3).

Optics EXPRESS

The proposed concept works not only for arrays of nanospheres but also for arrays of nanodisks (Fig. 3(a)), which can be readily produced by conventional nanofabrication approaches. A 2D map of $\Delta T = T_R - T_L$ for a zigzag chain of nanodisks (R_1, g = 100, 10 nm) is shown in Fig. 3(b). The small disk radius R_2 is changed from 0 to 100 nm, and the height (h) is fixed to 200 nm. The corresponding 2D maps of T_R and T_L are provided in Supplement 1 (Fig. S4). In analogy with the case of nanospheres, spin-dependent propagation is seen in the nanodisk chain since they also support similar Mie resonances. While the sphere system is simpler for understanding, the nanodisk system can be more advantageous in practice in terms of fabrication as well as for tailoring the optical properties with more degree of freedom in geometry, *i.e.* the height of the disks.

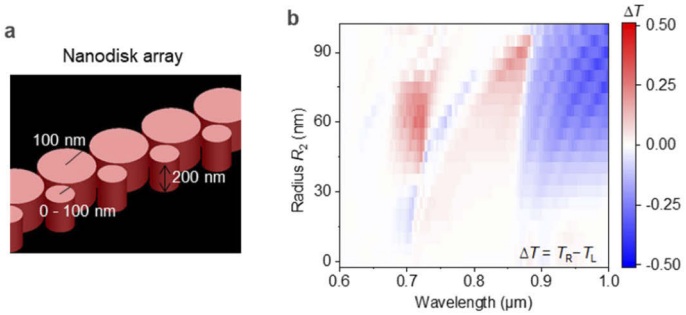

Fig. 3. Spin transport in asymmetric zigzag chains made of nanodisks (R_1, g) = (100, 10 nm). The height (h) is fixed to 200 nm. (a) Schematic illustration of the simulation geometries. As in the sphere cases, N = 31 is set and a σ^- circular dipole is positioned at the center of the chain for the excitation. (b) R_2 dependent transmission difference $\Delta T = T_R - T_L$. Individual T_R and T_L plots are provided in Fig. S4 in Supplement 1.

Next, we discuss the origin of the SLM behavior in the asymmetric zigzag chain. To this end, we present dispersion relations of the linear and asymmetric zigzag chains in Fig. 4. The ordinate and abscissa are a free-space wavenumber ($k_0 = 2\pi / \lambda$) and a Bloch wavenumber (β), respectively, normalized by a periodicity (a) and π. They are simulated for infinite chains using Bloch boundaries in the propagation direction (x-axis). Nonrelevant modes in the proposed system, *i.e.*, LM, LM', and TE_z' modes, are also included and plotted with orange curves. Mode profiles in panels b and d are calculated at a Bloch wavenumber $\beta a / \pi = 0.8$ and corresponding mode frequencies.

Figure 4(a) shows the dispersion relation of the linear chain. As can be seen, there are several guided modes below the light line. The field profiles in Fig. 4(b) allow us to assign the modes. In agreement with the previous reports [14,15,18], the first two modes from the low energy side are transverse-magnetic (TM) and longitudinal magnetic (LM) modes, where the magnetic dipole modes are transversely and longitudinally polarized, respectively. The abbreviation follows the convention. [15] The next two bands are transverse-electric (TE) and longitudinal-electric (LE) modes which originate from the electric dipole resonance. By comparing the bands of the dispersion relation with the transmission spectra shown in the side panels under excitation with either x- (green) or y- (purple) oriented linear or σ^- circular (red) dipoles, it is seen that the observed first and second transmission bands around 0.7 and 1.0 μm are dominated by LE and TM modes, respectively. LM mode does not appear in the transmission spectrum under the dipole excitation in the xy-plane due to a mismatch of symmetry.

In Fig. 4(c) and (d), the dispersion relations and mode profiles of the asymmetric zigzag chain are presented. The existent modes are not purely made of transverse/longitudinal electric/magnetic dipoles anymore, and thus they are distinguished in the notation from the symmetric chain with

Optics EXPRESS

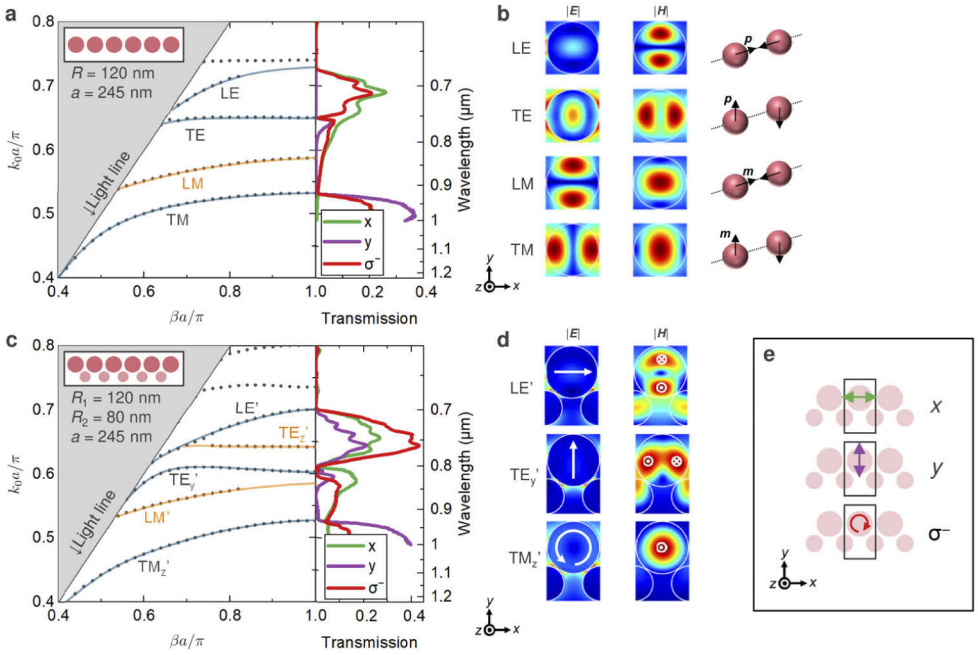

Fig. 4. Dispersion analysis of the guided modes. (a,c) Dispersion relation of (a) linear chain consisting of large nanoparticle (R, $g = 120$, 5 nm) and (c) Asymmetric zigzag chain with the basic parameter set (R_1, R_2, $g = 120$, 80, 5 nm). In both cases, the chains are infinitely long and have the same periodicity of 245 nm ($a = 2R_1 + g$). The shaded gray region shows the energy above the light line. On the right panels, corresponding transmission spectra (T_R) are shown. The definition of the excitation dipoles for transmission is shown in panel e. (b,d) Mode profiles at $\beta a / \pi = 0.8$ that correspond to panels a and c (left: electric field; right: magnetic field). The modes shown with orange curves in panels a and c cannot be excited in the geometry of transmission simulations due to a symmetry reason.

the primes. For example, the LE' mode has both LE and TE components due to the interaction with the side chain. For simplicity, we limit the discussion below to the modes that can be excited with a dipole oriented in the xy-plane (*i.e.,* bands traced by blue curves). The overall tendency is similar to the linear chain except for a slight low energy shift because of the increased modal volume. The relatively small deviation of the band structure, despite the perturbation of the mode profiles, is consistent with the non-degraded transmission efficiency in the asymmetric zigzag chain as discussed above. The dispersion relation reveals that the origin of the first transmission bands with SML can be attributed to the LE' mode. Likewise, the second band can be assigned to the TM_z' mode.

To obtain more physical insight into the SML in this system, we then discuss the spatial distribution of the transverse optical spin associated with the LE mode. The spin of structured optical fields can be described by SAM densities in the following formalism [25,26]:

$$\boldsymbol{s} = \mathrm{Im}[\varepsilon_0 \mu_r^{-1} \boldsymbol{E}^* \times \boldsymbol{E} + \mu_0 \varepsilon_r^{-1} \boldsymbol{H}^* \times \boldsymbol{H}]/4\omega. \tag{1}$$

This is the quantity responsible for the generation of SAM. The top panel of Fig. 5(a) shows an electric field profile ($|\boldsymbol{E}|$) of the LE mode ($\lambda = 0.71$ μm) of the linear chain on the xy-plane ($z = 0$) under excitation by a linear electric dipole with an orientation along the x-axis. Other electromagnetic field components (E_x, E_y, H_z) are presented in Supplement 1 (Fig. S5). It is seen that the launched field from the source at the central sphere counter-propagates to both sides.

Optics EXPRESS

Besides, the electric field is strongly confined around the line of $y = 0$. The normalized SAM density on the same plane is plotted in the bottom panel. Because E_z, H_x, and H_y are zero at $z = 0$, the SAM density is purely made of the electric component and is composed of s_z component in the plane. The red and blue colors in the plot indicate the opposite rotation directions of local fields (*i.e.,* up- and bottom-spins) when the light propagates. In this symmetric linear chain, the local spins are symmetrically distributed on both y-positive and negative sides albeit the opposite sign of the spin. In general, we can expect that local sources can efficiently couple to guided modes at the electric field maxima; however, the field distribution indicates that the local spin does not exist ($\boldsymbol{s} = 0$) at the electric field maximum at $y = 0$. In other words, ideal spots for spin coupling, where both $|\boldsymbol{E}|$ and $|\boldsymbol{s}|$ are both maximized, do not exist in the linear chain. Indeed, even if the source is placed at the SAM density maximum, the light transmission is significantly suppressed, leading to $\Delta T < 0.1$ in the LE mode (Fig. S6).

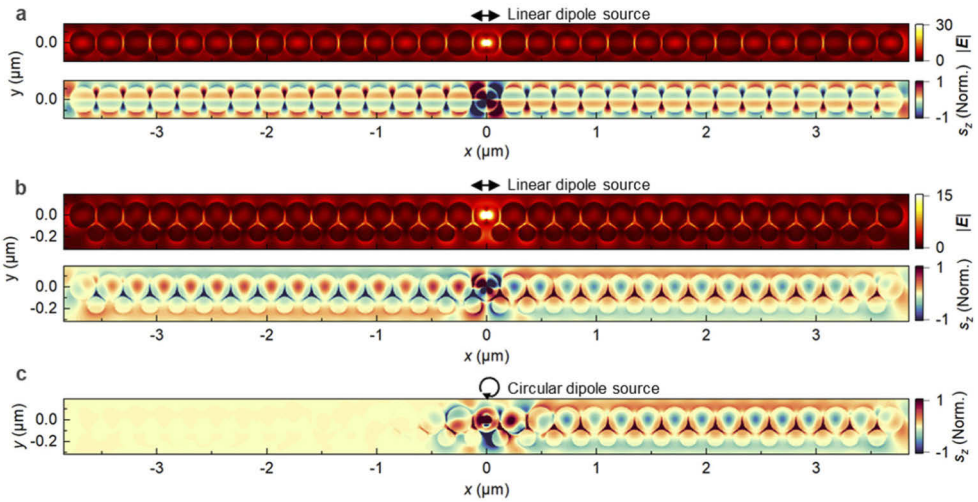

Fig. 5. Profiles of electric fields (top panels of a,b) and normalized spin densities (s_z; bottom panels of a,b and panel c) for (a) the linear chain (R, $g = 120$, 5 nm) and (b,c) asymmetric zigzag chain (R_1, R_2, $g = 120$, 80, 5 nm). The excitation source is (a,b) a x-oriented and (c) a σ^- circular electric dipole source. The intensity distribution for the circular dipole corresponds to the top panel of Fig. 1(d). The profiles at the wavelengths of the LE and LE' modes (a: $\lambda = 0.71$ μm; b,c: $\lambda = 0.76$ μm) are shown.

The electric field profile of the LE' mode ($\lambda = 0.76$ μm) of the asymmetric zigzag chain in the same geometry is shown in the top panel of Fig. 5(b). In stark contrast to the linear chain, the SAM density of the asymmetric zigzag chain in the bottom panel is not symmetrically distributed with respect to the xz-plane. On the right side of the chain (*i.e.,* for light propagating to the right), down-spins ($s_z < 0$) dominate the large sphere, while the gap region is dominated by up-spins ($s_z > 0$). This agrees with the observed directional SAM transport in Fig. 1, that is, the light from the σ^- dipole positioned in the large sphere selectively propagates to the right in the figure. In fact, an identical SAM density distribution can be seen in the right branch in Fig. 5(b) and (c). Moreover, the electric field maximum nicely overlaps the SAM density maximum at the center of the sphere. Thus, adding the side chain enables a spatial overlap of the high SAM density and field intensity (electromagnetic density of states), resulting in the efficient coupling of the rotating electric dipole to the guided mode.

In addition, the asymmetric zigzag chain offers accessible spots for efficient chiral light-matter coupling in the gap region between the large and small spheres with highly enhanced electric fields and SAM densities. As shown in Fig. S7, we see equivalently high transmission and directionality

Optics EXPRESS

under the excitation at the gap, while the transport direction is opposite. This provides an efficient and easily accessible coupling site to place light sources outside the structure, circumventing technical difficulties to embed quantum dots inside dielectric materials. [9,11,12,27]

Finally, we demonstrate the functionalities of the proposed chain. Figure 6(a) presents the spin transport over a curved chain with a bending radius of 2.5 μm. The directional transport in the anti-clockwise direction is clearly observed, though the electric field decays as it propagates compared to the straight chain. In contrast to photonic crystal waveguides, where the guiding direction is fixed to the crystal orientation, the truly 1D waveguide allows flexible bending in a continuous manner. In Fig. S8 (see Supplement 1), we provide the light-guiding over a sharp corner (~ 60°) in the first and second bands. The structural optimization would be the subject of future work, including the stability to 90° bending such as linear chains. [19]

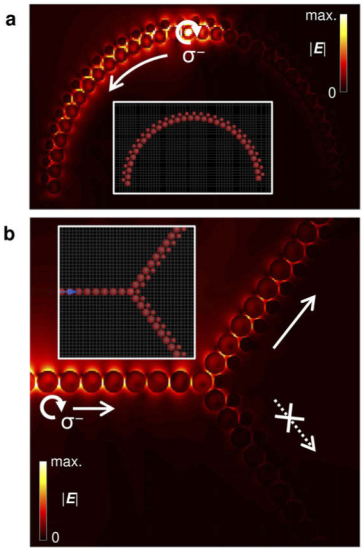

Fig. 6. Demonstration of functionalities of the asymmetric zigzag chain waveguide (R_1, R_2, g = 120, 80, 5 nm). (a) Directional light-guiding along a curved chain with a bending radius of 2.5 μm (λ = 0.764 μm). (b) Chiral light router, where the impinging light is routed to upper or lower branches depending on the circularity of the light (λ = 0.783 μm). The excitation source is a σ^- dipole.

In addition to the SML waveguiding, the introduction of asymmetry offers new functional elements that cannot be recognized in symmetric systems, for instance, an optical spin router (one-way splitter). As shown in Fig. 6(b), we design a star connection spin-router consisting of a linear chain as an input line and two lines of asymmetric zigzag chains as output ports. To generate the selectivity in light propagation depending on the transverse optical spins of impinging light, the asymmetric chains are arranged oppositely for upper and lower branches. The light source is a circular dipole in a linear chain, and σ^- polarized light is injected into the junction. Due to the asymmetric distribution of the SAM density in the asymmetric zigzag chain, light is routed to the upper branch. By switching the rotation of the source, the router branch is flipped to the bottom one. Similar junctions that selectively transport circular light into a certain direction have been reported in photonic crystal systems using an approach based on the topology. [28,29] The asymmetric zigzag chains miniaturize such devices down to a sub-wavelength scale, offering great compatibility with integrated photonics. In addition to this routing element, an optical spin isolator, that attenuates injected light of a certain parity (either up or down), can be realized by placing a damping element at one end.

Optics EXPRESS

3. Conclusion

In conclusion, we proposed an asymmetric zigzag chain made of silicon nanospheres or nanodisks as a novel platform for chiral light-matter interactions. Unlike previously studied waveguides whose symmetry is broken by the position of a light source or by an additional coupler, the chain inherently possesses SAM of light. Its large degree of freedom to design structure enables engineering of SAM densities for efficient couplings of local light sources at the electric field maxima. Furthermore, we proposed a novel design concept of spin device elements, such as an optical spin router. Our finding offers miniaturization of device footprints compared to previously reported similar systems based on photonic crystal waveguides (from $> 10\lambda$ to $\sim 0.5\lambda$), while propagation losses can instead be larger. To the best of our knowledge, this is the first report showing the SML phenomenon in chain systems. The proposed chain may be fabricated by assembling colloidal solutions of silicon nanospheres. [30–33] The nanodisk arrays are readily producible using standard nanofabrication technologies. Moreover, we expect the current perspective on Mie-tronics may be widely extended by shedding light on SML phenomena associated with Mie resonances. [34–37] For example, by arranging the proposed chain to constitute a metasurface, [38] efficient chiral sensing may be realized because up- and down-spins can be spatially separated.

4. Methods

The entire analysis was conducted using the FDTD method (FDTD Solutions; Lumerical/Ansys). The waveguides with finite lengths were modeled with silicon spheres arranged in a zigzag manner. Throughout this work, the existence of substrates was not considered, and all the spheres were positioned at $z = 0$. The simulation domain was defined by perfectly matched layers (PMLs) with a certain distance between the structure and the PMLs. The material dispersion of silicon was modeled by a built-in refractive index based on literature. [39] The spin-sorting performance of the chains was evaluated by light transmission at the rightmost (T_{R}) and leftmost (T_{L}) spheres, followed by normalization by the sum of transmission at the spheres one before and next to the source position.

Dispersion analysis was carried out for infinitely long waveguides using Bloch boundaries in the direction of light propagation. The other boundaries were terminated with PML boundaries. To excite all modes, the systems were excited by randomly distributed and oriented dipoles. The band structures were then derived in frequency-domain from time-domain signals captured by randomly distributed point monitors. The mode profiles were obtained in the same manner, except that either single or random dipoles were used to better visualize each mode.

Funding. Japan Society for the Promotion of Science (18J20276, 21H01782); Precursory Research for Embryonic Science and Technology (JPMJPR17P8); Murata Science Foundation.

Acknowledgments. T. Hinamoto acknowledges the support under Grant-in-Aid for JSPS Research Fellows.

Disclosures. The authors declare no conflicts of interest.

Data availability. Data underlying the results presented in this paper are not publicly available at this time but may be obtained from the authors upon reasonable request.

Supplemental document. See Supplement 1 for supporting content.

References

1. P. Lodahl, S. Mahmoodian, S. Stobbe, A. Rauschenbeutel, P. Schneeweiss, J. Volz, H. Pichler, and P. Zoller, "Chiral quantum optics," Nature **541**(7638), 473–480 (2017).
2. T. Van Mechelen and Z. Jacob, "Universal spin-momentum locking of evanescent waves," Optica **3**(2), 118–126 (2016).
3. S.-H. Gong, F. Alpeggiani, B. Sciacca, E. C. Garnett, and L. Kuipers, "Nanoscale chiral valley-photon interface through optical spin-orbit coupling," Science **359**(6374), 443–447 (2018).
4. P. Lodahl, S. Mahmoodian, and S. Stobbe, "Interfacing single photons and single quantum dots with photonic nanostructures," Rev. Mod. Phys. **87**(2), 347–400 (2015).

Optics EXPRESS

5. K. Y. Bliokh, A. Y. Bekshaev, and F. Nori, "Optical Momentum, Spin, and Angular Momentum in Dispersive Media," Phys. Rev. Lett. **119**(7), 073901 (2017).
6. D. O'Connor, P. Ginzburg, F. J. Rodríguez-Fortuño, G. A. Wurtz, and A. V. Zayats, "Spin–orbit coupling in surface plasmon scattering by nanostructures," Nat. Commun. **5**(1), 5327 (2014).
7. F. J. Rodriguez-Fortuno, G. Marino, P. Ginzburg, D. O'Connor, A. Martinez, G. a Wurtz, and A. V Zayats, "Near-field interference for the unidirectional excitation of electromagnetic guided modes," Science **340**(6130), 328–330 (2013).
8. J. Petersen, J. Volz, and A. Rauschenbeutel, "Chiral nanophotonic waveguide interface based on spin-orbit interaction of light," Science **346**(6205), 67–71 (2014).
9. R. J. Coles, D. M. Price, J. E. Dixon, B. Royall, E. Clarke, P. Kok, M. S. Skolnick, A. M. Fox, and M. N. Makhonin, "Chirality of nanophotonic waveguide with embedded quantum emitter for unidirectional spin transfer," Nat. Commun. **7**(1), 11183 (2016).
10. A. Javadi, D. Ding, M. H. Appel, S. Mahmoodian, M. C. Löbl, I. Söllner, R. Schott, C. Papon, T. Pregnolato, S. Stobbe, L. Midolo, T. Schröder, A. D. Wieck, A. Ludwig, R. J. Warburton, and P. Lodahl, "Spin–photon interface and spin-controlled photon switching in a nanobeam waveguide," Nat. Nanotechnol. **13**(5), 398–403 (2018).
11. I. J. Luxmoore, N. A. Wasley, A. J. Ramsay, A. C. T. Thijssen, R. Oulton, M. Hugues, A. M. Fox, and M. S. Skolnick, "Optical control of the emission direction of a quantum dot," Appl. Phys. Lett. **103**(24), 241102 (2013).
12. I. Söllner, S. Mahmoodian, S. L. Hansen, L. Midolo, A. Javadi, G. Kiršanskė, T. Pregnolato, H. El-Ella, E. H. Lee, J. D. Song, S. Stobbe, and P. Lodahl, "Deterministic photon–emitter coupling in chiral photonic circuits," Nat. Nanotechnol. **10**(9), 775–778 (2015).
13. B. le Feber, N. Rotenberg, and L. Kuipers, "Nanophotonic control of circular dipole emission," Nat. Commun. **6**(1), 6695 (2015).
14. R. M. Bakker, Y. F. Yu, R. Paniagua-Domínguez, B. Luk'yanchuk, and A. I. Kuznetsov, "Resonant light guiding along a chain of silicon nanoparticles," Nano Lett. **17**(6), 3458–3464 (2017).
15. R. S. Savelev, A. P. Slobozhanyuk, A. E. Miroshnichenko, Y. S. Kivshar, and P. A. Belov, "Subwavelength waveguides composed of dielectric nanoparticles," Phys. Rev. B **89**(3), 035435 (2014).
16. L. Ding, D. Morits, R. Bakker, S. Li, D. Eschimese, S. Zhu, Y. F. Yu, R. Paniagua-Dominguez, and A. I. Kuznetsov, "All-optical modulation in chains of silicon nanoantennas," ACS Photonics **7**(4), 1001–1008 (2020).
17. L. Ding, Y. F. Yu, D. Morits, M. Yu, T. Y. L. Ang, H.-S. Chu, S. Thor Lim, C. E. Png, R. Paniagua-Dominguez, and A. I. Kuznetsov, "Low loss waveguiding and slow light modes in coupled subwavelength silicon Mie resonators," Nanoscale **12**(42), 21713–21718 (2020).
18. R. S. Savelev, D. S. Filonov, M. I. Petrov, A. E. Krasnok, P. A. Belov, and Y. S. Kivshar, "Resonant transmission of light in chains of high-index dielectric particles," Phys. Rev. B **92**(15), 155415 (2015).
19. R. S. Savelev, D. S. Filonov, P. V. Kapitanova, A. E. Krasnok, A. E. Miroshnichenko, P. A. Belov, and Y. S. Kivshar, "Bending of electromagnetic waves in all-dielectric particle array waveguides," Appl. Phys. Lett. **105**(18), 181116 (2014).
20. J. Du, S. Liu, Z. Lin, J. Zi, and S. T. Chui, "Guiding electromagnetic energy below the diffraction limit with dielectric particle arrays," Phys. Rev. A **79**(5), 051801 (2009).
21. J. Du, S. Liu, Z. Lin, J. Zi, and S. T. Chui, "Dielectric-based extremely-low-loss subwavelength-light transport at the nanoscale: An alternative to surface-plasmon-mediated waveguiding," Phys. Rev. A **83**(3), 035803 (2011).
22. R. S. Savelev, A. V. Yulin, A. E. Krasnok, and Y. S. Kivshar, "Solitary waves in chains of high-index dielectric nanoparticles," ACS Photonics **3**(10), 1869–1876 (2016).
23. A. P. Slobozhanyuk, A. N. Poddubny, I. S. Sinev, A. K. Samusev, Y. F. Yu, A. I. Kuznetsov, A. E. Miroshnichenko, and Y. S. Kivshar, "Enhanced photonic spin Hall effect with subwavelength topological edge states," Laser & Photonics Reviews **10**(4), 656–664 (2016).
24. F. N. Gür, C. P. T. McPolin, S. Raza, M. Mayer, D. J. Roth, A. M. Steiner, M. Löffler, A. Fery, M. L. Brongersma, A. V. Zayats, T. A. F. König, and T. L. Schmidt, "DNA-assembled plasmonic waveguides for nanoscale light propagation to a fluorescent nanodiamond," Nano Lett. **18**(11), 7323–7329 (2018).
25. D. R. Abujetas and J. A. Sánchez-Gil, "Spin angular momentum of guided light induced by transverse confinement and intrinsic helicity," ACS Photonics **7**(2), 534–545 (2020).
26. K. Y. Bliokh, A. Y. Bekshaev, and F. Nori, "Extraordinary momentum and spin in evanescent waves," Nat. Commun. **5**(1), 3300 (2014).
27. M. Arcari, I. Söllner, A. Javadi, S. Lindskov Hansen, S. Mahmoodian, J. Liu, H. Thyrrestrup, E. H. Lee, J. D. Song, S. Stobbe, and P. Lodahl, "Near-unity coupling efficiency of a quantum emitter to a photonic crystal waveguide," Phys. Rev. Lett. **113**(9), 093603 (2014).
28. C. He, X.-L. Chen, M.-H. Lu, X.-F. Li, W.-W. Wan, X.-S. Qian, R.-C. Yin, and Y.-F. Chen, "Tunable one-way cross-waveguide splitter based on gyromagnetic photonic crystal," Appl. Phys. Lett. **96**(11), 111111 (2010).
29. Z. Yu, G. Veronis, Z. Wang, and S. Fan, "One-way electromagnetic waveguide formed at the interface between a plasmonic metal under a static magnetic field and a photonic crystal," Phys. Rev. Lett. **100**(2), 023902 (2008).
30. T. Hinamoto, S. Hotta, H. Sugimoto, and M. Fujii, "Colloidal solutions of silicon nanospheres toward all-dielectric optical metafluids," Nano Lett. **20**(10), 7737–7743 (2020).
31. H. Sugimoto and M. Fujii, "Colloidal dispersion of subquarter micrometer silicon spheres for low-loss antenna in visible regime," Adv. Opt. Mater. **5**(17), 1700332 (2017).

Optics EXPRESS

32. H. Sugimoto, T. Okazaki, and M. Fujii, "Mie resonator color inks of monodispersed and perfectly spherical crystalline silicon nanoparticles," Adv. Opt. Mater. **8**(12), 2000033 (2020).
33. H. Sugimoto, T. Hinamoto, and M. Fujii, "Forward to backward scattering ratio of dielectric–metal heterodimer suspended in almost free-space," Adv. Opt. Mater. **7**(20), 1900591 (2019).
34. T. Matsukata, F. J. García de Abajo, and T. Sannomiya, "Chiral light emission from a sphere revealed by nanoscale relative-phase mapping," ACS Nano **15**(2), 2219–2228 (2021).
35. R. Won, "Into the 'Mie-tronic' era," Nat. Photonics **13**(9), 585–587 (2019).
36. T. Matsukata, N. Matthaiakakis, T. Yano, M. Hada, T. Tanaka, N. Yamamoto, and T. Sannomiya, "Selection and visualization of degenerate magnetic and electric multipoles up to radial higher orders by cathodoluminescence," ACS Photonics **6**(9), 2320–2326 (2019).
37. A. I. Kuznetsov, A. E. Miroshnichenko, M. L. Brongersma, Y. S. Kivshar, and B. Luk'yanchuk, "Optically resonant dielectric nanostructures," Science **354**(6314), aag2472 (2016).
38. L. Sun, C. Y. Wang, A. Krasnok, J. Choi, J. Shi, J. S. Gomez-Diaz, A. Zepeda, S. Gwo, C. K. Shih, A. Alù, and X. Li, "Separation of valley excitons in a MoS 2 monolayer using a subwavelength asymmetric groove array," Nat. Photonics **13**(3), 180–184 (2019).
39. Edward D. Palik, *Handbook of Optical Constants of Solids* (Academic University, 1998).